Monthly Notices of the ROYAL ASTRONOMICAL SOCIETY

MNRAS **526,** 1940–1950 (2023) https://doi.org/10.1093/mnras/stad2790
Advance Access publication 2023 September 14

Molecular and ionized gas in tidal dwarf galaxies: the spatially resolved star formation relation

N. Kovakkuni,[1★] F. Lelli,[2★] P.-A. Duc,[3] M. Boquien,[4] J. Braine,[5] E. Brinks,[6] V. Charmandaris,[7,8,9] F. Combes,[10] J. Fensch,[11] U. Lisenfeld,[12,13] S. S. McGaugh,[14] J. C. Mihos,[14] M. S. Pawlowski,[15] Y. Revaz[16] and P. M. Weilbacher[15]

[1]*Centro de Astronomía (CITEVA), Universidad de Antofagasta, Avenida Angamos 601, Antofagasta, Chile*
[2]*INAF, Arcetri Astrophysical Observatory, Largo Enrico Fermi 5, I-50125 Florence, Italy*
[3]*Observatoire astronomique de Strasbourg (ObAS), Université de Strasbourg, CNRS, UMR 7550, F-67000 Strasbourg, France*
[4]*Instituto de Alta Investigación, Universidad de Tarapacá, Casilla 7D, Arica, Chile*
[5]*Laboratoire d'Astrophysique de Bordeaux, Univ. Bordeaux, CNRS, B18N, allée Geoffroy Saint-Hilaire, F-33615 Pessac, France*
[6]*Centre for Astrophysics Research, University of Hertfordshire, College Lane, Hatfield AL10 9AB, UK*
[7]*Department of Physics, University of Crete, Heraklion 71003, Greece*
[8]*Institute of Astrophysics, Foundation for Research and Technology-Hellas (FORTH), Heraklion 70013, Greece*
[9]*School of Sciences, European University Cyprus, Diogenes street, Engomi, Nicosia 1516, Cyprus*
[10]*LERMA, Observatoire de Paris, PSL Research Université, CNRS, Sorbonne Université, UPMC, 61, avenue de l'Observatoire - F-75014 Paris, France*
[11]*Centre de Recherche Astrophysique de Lyon, Univ. Lyon, ENS de Lyon, Univ. Lyon 1, CNRS, UMR5574, F-69007 Lyon, France*
[12]*Departamento de Física Teórica y del Cosmos, Universidad de Granada, E-18071 Granada, Spain*
[13]*Facultad de Ciencias, Instituto Carlos I de Fisica Teorica y Computacional, E-18071 Granada, Spain*
[14]*Department of Astronomy, Case Western Reserve University, Cleveland, OH 44106, USA*
[15]*Leibniz-Institut für Astrophysik Potsdam (AIP), An der Sternwarte 16, D-14482 Potsdam, Germany*
[16]*Institute of Physics, Laboratory of Astrophysics, École Polytechnique Fédérale de Lausanne (EPFL), CH-1290 Sauverny, Switzerland*

Accepted 2023 September 8. Received 2023 September 5; in original form 2023 May 25

ABSTRACT

Tidal dwarf galaxies (TDGs) are low-mass objects that form within tidal and/or collisional debris ejected from more massive interacting galaxies. We use CO(1–0) observations from Atacama Large Millimeter/submillimeter Array and integral-field spectroscopy from Multi-Unit Spectroscopic Explorer to study molecular and ionized gas in three TDGs: two around the collisional galaxy NGC 5291 and one in the late-stage merger NGC 7252. The CO and H α emission is more compact than the H I emission and displaced from the H I dynamical centre, so these gas phases cannot be used to study the internal dynamics of TDGs. We use CO, H I, and H α data to measure the surface densities of molecular gas ($\Sigma_{\rm mol}$), atomic gas ($\Sigma_{\rm atom}$), and star formation rate ($\Sigma_{\rm SFR}$), respectively. We confirm that TDGs follow the same spatially integrated $\Sigma_{\rm SFR}$–$\Sigma_{\rm gas}$ relation of regular galaxies, where $\Sigma_{\rm gas} = \Sigma_{\rm mol} + \Sigma_{\rm atom}$, even though they are H I dominated. We find a more complex behaviour in terms of the spatially resolved $\Sigma_{\rm SFR}$–$\Sigma_{\rm mol}$ relation on subkpc scales. The majority ($\sim$ 60 per cent) of star-forming regions in TDGs lie on the same $\Sigma_{\rm SFR}$–$\Sigma_{\rm mol}$ relation of normal spiral galaxies but show a higher dispersion around the mean. The remaining fraction of star-forming regions ($\sim$ 40 per cent) lie in the starburst region and are associated with the formation of massive super star clusters, as shown by *Hubble Space Telescope* images. We conclude that the local star formation activity in TDGs proceeds in a hybrid fashion, with some regions comparable to normal spiral galaxies and others to extreme starbursts.

Key words: galaxies: dwarf – galaxies: evolution – galaxies: formation – galaxies: interactions – galaxies: ISM – galaxies: star formation.

1 INTRODUCTION

The process of star formation (SF) plays a key role in the formation and evolution of galaxies. Key insights into the SF process are given by empirical relations that connect the star formation rate (SFR) of a galaxy to the availability of gas in the interstellar medium (ISM). One such relation is the Kennicutt–Schmidt (KS) relation. In its original form, the Schmidt (1959) relation connected volume densities of SFR ($\rho_{\rm SFR}$) and atomic gas mass ($\rho_{\rm HI}$) in star-forming regions of the Milky Way:

$$\rho_{\rm SFR} \propto \rho_{\rm H\,I}^{n}. \quad (1)$$

Subsequent studies (Kennicutt 1998b) of star-forming galaxies revealed a tight relation between the disc-averaged SFR surface densities ($\Sigma_{\rm SFR}$) and total (atomic plus molecular) gas mass surface densities ($\Sigma_{\rm gas}$):

$$\Sigma_{\rm SFR} = A\,\Sigma_{\rm gas}^{N}. \quad (2)$$

★ E-mail: navyasree.kovakkuni@ua.cl (NK); federico.lelli@inaf.it (FL)

With the advent of multiwavelength observations at high angular resolution, it has become possible to study the KS relation in a spatially resolved fashion on kpc-scales in a variety of environments, from spiral galaxies to interacting objects (e.g. Bigiel et al. 2008; Leroy et al. 2008; Boquien et al. 2011). These works suggested that the SFR surface density correlates more strongly with molecular gas (H_2) than atomic gas in the inner H_2-dominated regions of star-forming discs. The situation, however, remains unclear in the H I-dominated regime, typical of dwarf galaxies (Roychowdhury et al. 2014, 2015) as well as the outermost parts of spiral galaxies (Bigiel et al. 2010). In this regime, flares in the outer gaseous discs (i.e. a radial increase of the disc thickness) may play an important role (Bacchini et al. 2019, 2020), suggesting that the volume density of total gas (atomic plus molecular) best correlates with the volume density of SFR, in analogy to the original form in equation (1).

A key question is whether every galaxy follows the same KS relation, thus whether the SF process is 'universal' or not on subkpc scales. For example, there is a clear link between SF activity and galaxy interactions (e.g. Ellison et al. 2013). Tidal interactions lead to gas inflows towards the galaxy centres, which can temporarily enhance the SFRs, and move the resulting systems above the mean KS relation in the so-called starburst regime (e.g. Barnes & Hernquist 1991; Renaud et al. 2014; Ellison et al. 2020). At the same time, galaxy collisions expel gas and stars into intergalactic space, leading to the formation of tails and bridges in which new stars can form. SF, indeed, can occur within gas debris surrounding interacting systems, sometimes even at 100 kpc away from the parent galaxies (Mirabel, Dottori & Lutz 1992; Duc, Bournaud & Boquien 2006; Boquien et al. 2007, 2011). Is the SF occurring in such extreme environments proceeding in a similar way as in galaxy discs?

Tidal dwarf galaxies (TDGs) are self-gravitating objects found within tidal debris, which show *in situ* SF and have masses and sizes comparable to 'normal' dwarf galaxies (Duc et al. 2006). Zwicky (1956) was the first to suggest the possible formation of TDGs around interacting galaxies; this hypothesis was later confirmed by several observational and theoretical studies (e.g. Barnes & Hernquist 1992; Mirabel et al. 1992; Elmegreen, Kaufman & Thomasson 1993). Hereafter, for simplicity, we will use the term TDG to also include newborn galaxies that form within collisional debris (rather than tidal ones), such as the SF complexes in the collisional ring of NGC 5291 (Bournaud et al. 2007). In addition, we will refer to 'bona-fide TDGs' to indicate systems that show internal kinematics decoupled from the surrounding debris, pointing to self-gravity within a local potential well (e.g. Lelli et al. 2015). Bona-fide TDGs have been identified around several interacting systems (e.g. Duc et al. 2006; Lelli et al. 2015).

TDGs form out of gas that has been pre-enriched in their parent massive galaxies, giving them higher gas-phase metallicities (about 0.3–0.5$Z_\odot$) than 'classical' dwarf galaxies (Duc & Mirabel 1998). Thus, contrarily to most dwarf galaxies, TDGs are easily detected in the CO emission line, and it is sensible to use the Milky Way X_{CO} factor to convert the observed CO flux density into H_2 column densities (Braine et al. 2001; Lisenfeld et al. 2016; Querejeta et al. 2021). Braine et al. (2001) used single-dish CO observations of eight TDGs to conclude that they follow the same galaxy-averaged KS relation of usual galaxies. Boquien et al. (2011) reached the same conclusion for a TDG candidate in the interacting system Arp 158. On the other hand, Lisenfeld et al. (2016) presented a spatially resolved study of a TDG in the Virgo Cluster and found that it lies below the mean KS relation. Finally, Querejeta et al. (2021) analysed high-resolution Atacama Large Millimeter/submillimeter Array (ALMA) observations of a TDG in the interacting system Arp 94, and found that it may lie either on or off the KS relation, depending on whether one considers the whole CO flux or only the one associated with giant molecular clouds. The diverse outcome of these works may point to different behaviour in the galaxy-averaged and spatially resolved KS relation and/or intrinsic differences in the SF properties of individual TDGs, potentially related to their different formation and evolutionary histories. New studies are needed to clarify the situation.

In this paper, we study the spatially resolved KS relation in a sample of three TDGs: NGC 5291N, NGC 5291S, and NGC 7252NW. We probe their molecular gas content using CO(1–0) observations from the ALMA, and their ionized gas content (Hα and Hβ emission) using integral-field spectroscopy (IFS) from the Multi-Unit Spectroscopic Explorer (MUSE) mounted on the Very Large Telescope (VLT). New observations and ancillary data are described in Section 2. Results on the gas distribution and kinematics as well as on the KS relation are presented in Section 3. Finally, we summarize our findings in Section 4

2 OBSERVATIONS

2.1 Galaxy sample

We obtained high-resolution ALMA observations for three TDGs that were selected from the sample of Lelli et al. (2015), based on the availability of single-dish CO fluxes and high-quality H I maps. Two of them are part of the NGC 5291 system; the remaining one is part of the NGC 7252 merger. The location of these TDGs within the overall structure of the parent system can be appreciated in fig. 1 of Lelli et al. (2015). Table 1 lists the general properties of these TDGs.

NGC 5291 is a perturbed early-type galaxy that is surrounded by a giant H I ring (Malphrus et al. 1997), suggesting a past head-on collision (Bournaud et al. 2007). The system is located in the outer region of the galaxy cluster Abell 3574. Early studies by Longmore et al. (1979) in the collisional ring of NGC 5291 revealed the presence of star-forming regions out to 100 kpc from the central galaxy. Subsequently, Duc & Mirabel (1998) found that these star-forming complexes have similar sizes and SFRs of dwarf galaxies but higher metallicities, suggesting a TDG origin. Three star-forming complexes (NGC 5291N, NGC 5291S, and NGC 5291SW) are associated with strong H I concentrations that display a velocity gradient decoupled from the underlying collisional material, pointing to rotation within a self-gravitating potential well (Bournaud et al. 2007; Lelli et al. 2015). In this paper, we focus on NGC 5291N and NGC 5291S because no single-dish CO observations are available for NGC 5291SW.

NGC 7252 (also known as 'Atoms for Peace') is a late-stage merger remnant with two gas-rich tidal tails extending to the east and north–west. Numerical simulations (Borne & Richstone 1991; Hibbard & Mihos 1995; Chien & Barnes 2010) were able to reproduce the observed morphology and kinematics of NGC 7252 from the merging of two disc galaxies. Hibbard et al. (1994) identified two TDG candidates in the North-Western and Eastern tails (NGC 7252NW and NGC 7252E). These star-forming complexes were confirmed as bona-fide TDGs based on their Hα kinematics (Bournaud et al. 2004), H I kinematics (Lelli et al. 2015), and relatively high gas metallicities (Lelli et al. 2015). In this paper, we focus on NGC 7252NW because no single-dish CO observations are available for NGC 7252SE.

Table 1. TDG sample. Distances are adopted from Lelli et al. (2015). Redshifts and systemic velocities are computed from Hα emission lines (Section 3.2). SFRs, molecular gas masses, and atomic gas masses are computed within the total CO emitting area, but the TDG size is significantly larger (see Section 3.3 for details).

Galaxy	RA (J2000)	Dec. (J2000)	Dist. (Mpc)	z	V_{sys} (km s^{-1})	SFR ($M_\odot$ yr^{-1})	M_{mol} (10^7 $M_\odot$)	M_{atom} (10^7 $M_\odot$)	Area (kpc^2)
NGC 5291N	13 47 20.3	−30 20 54	62	0.014	4228.8	0.6 ± 0.1	5.5 ± 1.1	163.6 ± 16.7	25.0
NGC 5291S	13 47 22.7	−30 27 40	62	0.016	4780.4	0.2 ± 0.1	2.6 ± 0.4	124.1 ± 16.1	16.0
NGC 7252NW	22 20 33.7	−24 37 24	66.5	0.016	4771.6	0.06 ± 0.02	3.2 ± 0.6	11.7 ± 2.2	12.3

Table 2. Properties of CO data cubes with a channel width of ∼5 km s^{-1}.

Galaxy	Beam (arcsec × arcsec)	Beam PA (deg)	σ_{cube} (mJy beam^{-1})
NGC 5291N	2.1 × 1.7	75.5	0.5
NGC 5291S	2.1 × 1.8	−4.6	0.5
NGC 7252NW	2.7 × 1.6	−8.3	0.5

2.2 ALMA data

The three TDGs were observed by the ALMA 12m array in 2016 January (Project 2015.1.00645.S; PI: F. Lelli). The time on source was about 2.2 h for both NGC 5291N and NGC 5291S, and about 4.5 h for NGC 7252NW. We used ALMA band 3 with a mixed spectral set-up, using four spectral windows with a bandwidth of 1875 MHz each. A high-resolution spectral window was centred at the frequency of the redshifted CO(1–0) line and covered with 3480 channels, providing a spectral resolution of 976.6 kHz (∼2.6 km s^{-1}). Three low-resolution spectral windows were centred around 99, 100, and 110 GHz to target the mm continuum; they were covered with 128 channels providing a spectral resolution of 31.250 MHz (ranging from ∼84 to ∼94 km s^{-1}). The observations were pointed at the H I kinematic centre of the TDGs and have a field of view of ∼50 arcsec, set by the full width at half-maximum (FWHM) of the primary beam.

The data reduction was performed with the COMMON ASTRONOMY SOFTWARE APPLICATIONS (CASA) package (McMullin et al. 2007). The *uv* data were flagged and calibrated using the standard CASA pipeline. Both continuum and line data were imaged using the `tclean` task with a Högbom deconvolver and Briggs weighting with a robust parameter of 0.5. Continuum images were constructed by combining all four spectral windows, excluding channels with line emission. Continuum emission was detected only in NGC 5291NW and subtracted from the CO(1–0) line channels using the task `uvcontsub`. The properties of the CO(1–0) line cubes are summarized in Table 2. In particular, the spatial resolution (FWHM of the synthesized beam) is about 2 arcsec that corresponds to about 600 and 650 pc at the distances of NGC 5291 and NGC 7252, respectively.

CO intensity (moment-zero) maps were constructed by summing channels with CO emission and are shown in Fig. 1. They are discussed in Section 3.1 for illustrative purpose only: CO fluxes are measured by extracting integrated spectra in various spatial regions as described in Section 3.2. No corrections for the primary beam are applied in the moment maps, instead they are applied to the derived fluxes as described in Section 3.2. Since the ALMA primary beam is significantly larger than the CO emitting area, the primary beam attenuation has little effect on the moment-zero maps, with the exception of NGC 5291S. For this TDG, the pointing centre was chosen in-between two main SF complexes so that the CO emission in the Northern complex (the Southern is not detected) is ∼10 arcsec offset from the pointing centre (see Fig. 1). It is also possible that the two SF complexes are two distinct objects, whose individual kinematics cannot be discerned with the available H I observations (Lelli et al. 2015). Correction for primary beam attenuation is described in Section 3.2.

The CO emission is very compact and confined to one or two major clumps that display no appreciable velocity gradients (Fig. 1), so moment-one and moment-two maps are not very useful. We will discuss the CO kinematics using position-velocity (PV) diagrams that provide the most direct representation of the 3D data (Section 3.1). Before extracting integrated spectra, to enhance the signal-to-noise (S/N) ratio of the CO line, we performed Hanning smoothing over three spectral channels, giving a final velocity resolution of ∼10 km s^{-1}.

To investigate whether the ALMA interferometric observations may be missing diffuse flux on large scales, we compared spatially integrated CO spectra from ALMA with those from previous single-dish observations (Braine et al. 2001). The low S/N of the previous single-dish observations do not allow us to quantify the amount of diffuse molecular gas missed by the ALMA interferometric observations. The comparison therefore was inconclusive, but we note that a substantial amount of diffuse CO emission has been found in another TDG (J1023+1952) using ALMA total power (TP) and Atacama Compact Array (ACA) observations in addition to the 12 m array (Querejeta et al. 2021). It is possible therefore that our high-resolution observations are probing only the densest CO emission and may be missing some flux on larger scales. ACA and TP observations (or deep IRAM-30 observations) are needed to check this possibility.

2.3 MUSE data

NGC 5291N was observed on 2014 June 26 (Program ID: 60.A-9320; PI: P.-A. Duc) without adaptive optics (AO) for a total exposure time of 1800 s. These observations are presented in Fensch et al. (2016), who provides an in-depth study of line ratios and gas metallicity. NGC 5291N was re-observed on 2017 June 19 during a MUSE AO commissioning run (Program ID: 60.A-9100(G)), but the AO system could not significantly improve on the external seeing, so we will not use these data.

NGC 5291S was observed on 2018 January 22 as part of Program ID 097.B-0152 (PI: M. Boquien) without AO for a total exposure time of 1800 s. NGC 7252NW was observed on 2017 July 16 during a commissioning run of the MUSE AO wide-field mode (Program ID: 60.A-9100(H)) for a total exposure time of 900 s. All data were reduced using the MUSE pipeline v2.4 and following standard procedures (Weilbacher et al. 2020). For NGC 5291S, the sky was estimated using an offset field, while for NGC 7252NW, it was estimated within the science exposure. We refer to Fensch et al. (2016) for further details on the data reduction.

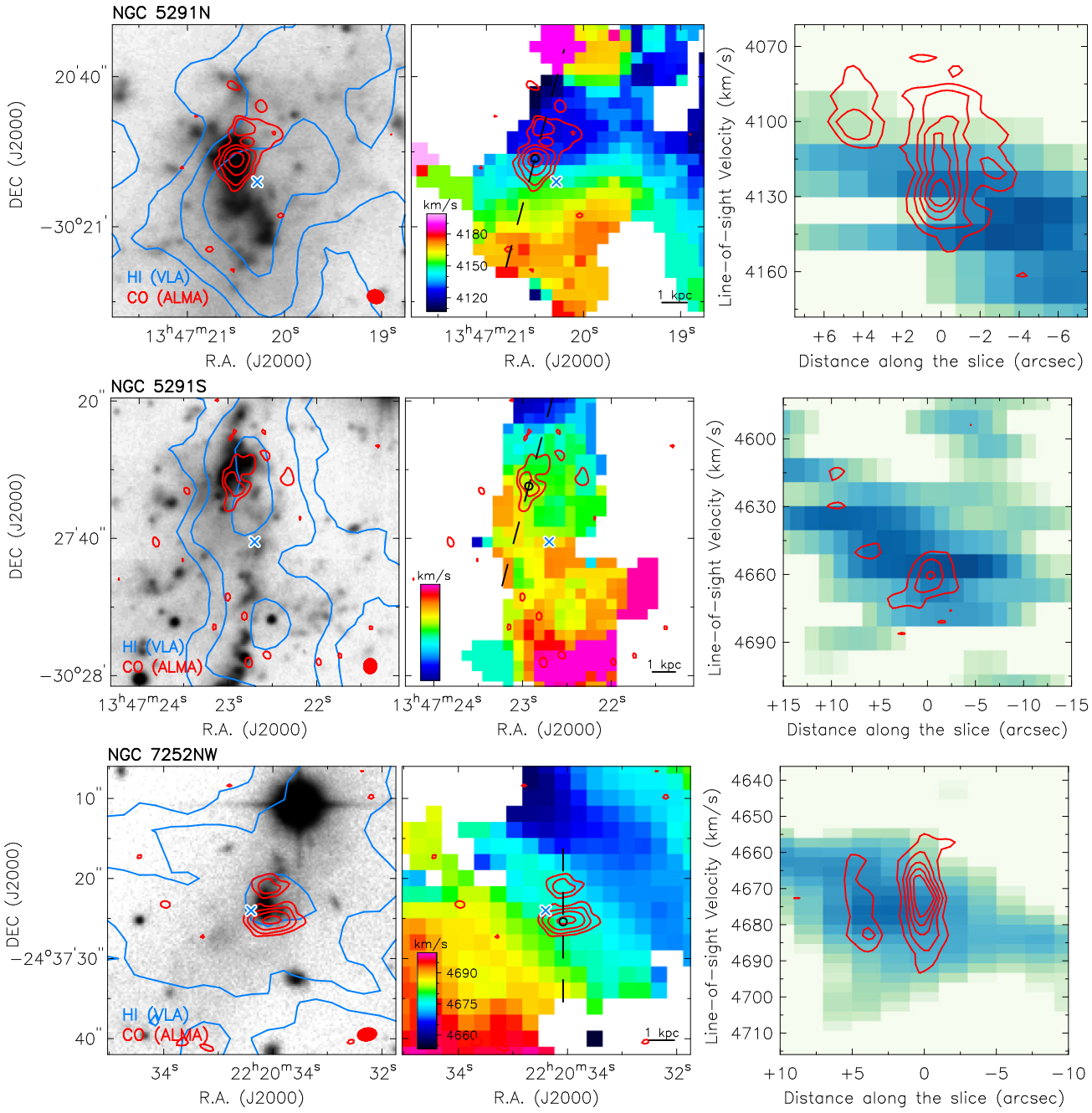

Figure 1. Gas distribution and kinematics in NGC 5291N (top), NGC 5291S (middle), and NGC 7252NW (bottom). In all panels, the CO(1–0) data are from this work, while the other data come from Lelli et al. (2015). *Left panels:* Optical *R*-band image overlaid with the H I map (blue contours) and the CO(1–0) map (red contours). H I contours are the same as in Lelli et al. (2015). CO contours are at (3, 6, 12, 24) $\sigma_{\rm map}$, where $\sigma_{\rm map} = 0.02$ Jy beam^{-1} km s^{-1} for NGC 7252NW and $\sigma_{\rm map} = 0.03$ Jy beam^{-1} km s^{-1} for both NGC 5291N and NGC 5291S. The cross shows the H I kinematic centre that was chosen as the ALMA pointing centre. The ALMA beam is shown by the red ellipse to the bottom right corner; the H I beam (not shown) is about 4 times larger for NGC 5291 and 6 times for NGC 7252. *Middle panels:* H I velocity field overlaid with the CO map. The dashed line shows the slit used to extract the PV diagram. The physical scale of 1 kpc is indicated by the bar in the bottom right corner. *Right panels*: PV diagrams from the H I cube (blue colourscale) overlaid with those from the CO cube (red contours). CO contours range from $3\sigma_{\rm cube}$ to $15\sigma_{\rm cube}$ in steps of $3\sigma_{\rm cube}$ (see Table 2).

Moment-zero maps were constructed by summing channels with Hα and Hβ emission. These maps are intended to show the morphology of the ionized gas; line fluxes will be measured by extracting integrated spectra and subtracting the stellar continuum (Section 3.2).

3 RESULTS

3.1 Distribution and kinematics of multiphase gas

Fig. 1 compares the distribution and kinematics of molecular (CO) and atomic (H I) gas in our sampled TDGs. In all galaxies, the

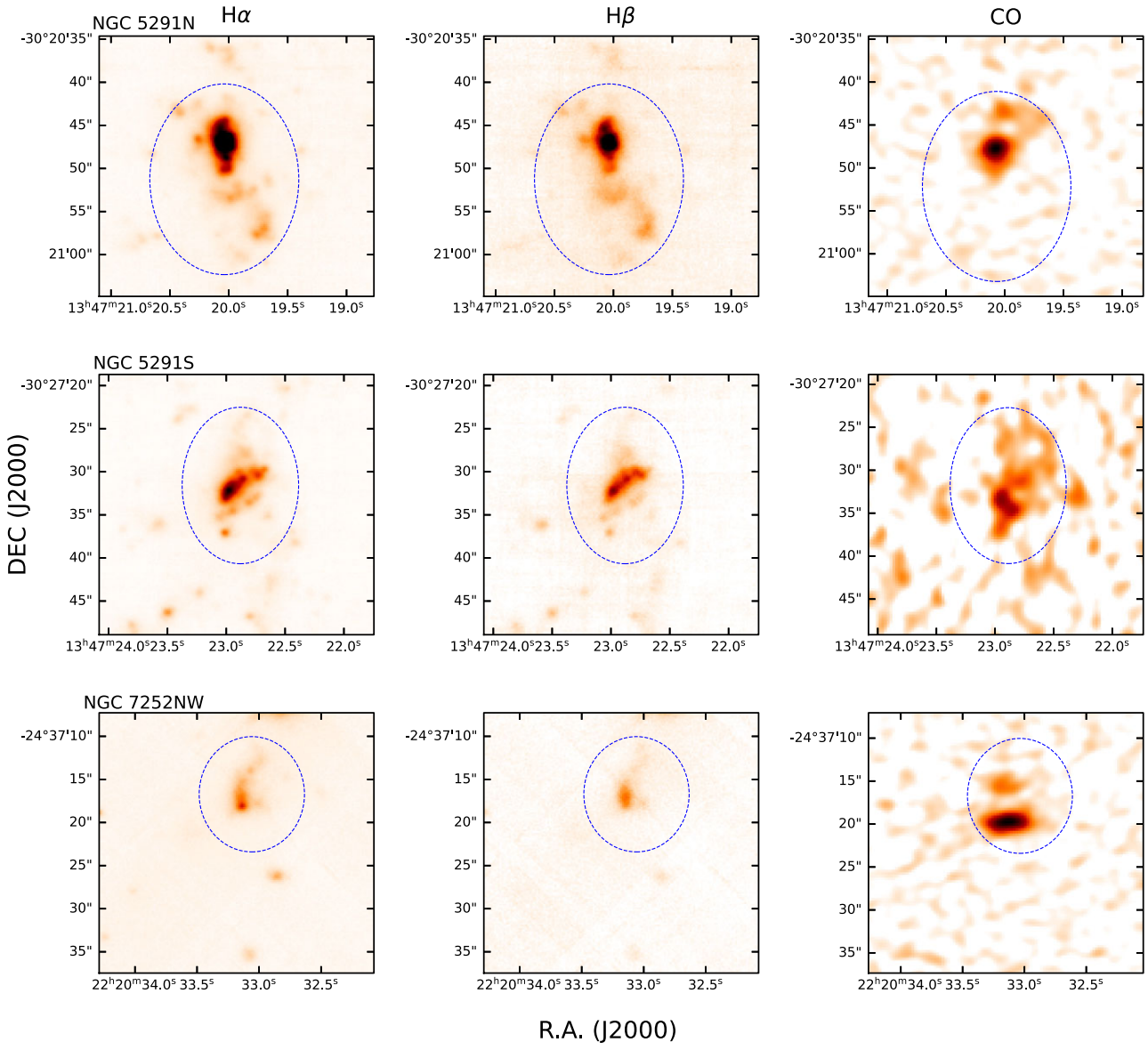

Figure 2. Spatial distribution of H α (left), H β (middle), and CO(1–0) velocity-integrated emission (right) in NGC 5291N (top), NGC 5291S (middle), and NGC 7252NW (bottom). The elliptical area marked with blue dashed line shows the integration region used to compute the total H α, H β, and CO fluxes of the TDGs.

detected CO emission is much more compact than the H I emission (left panels) and associated with intense SF, as we describe later on. The CO extent is of the order of 1–2 kpc, while the H I discs have diameters ranging from ∼10 to ∼15 kpc (Lelli et al. 2015). The CO emission lies near the edges of the H I peaks, so there is no direct correspondence between the atomic and molecular gas distribution on kpc scales. Moreover, the CO emission is not at the dynamical centre of the TDGs, so it cannot be used to trace the underlying large-scale gas rotation (middle panels). The same behaviour is often seen in typical dwarfs and in the outskirts of spirals, where the H I emission traces the object more globally, and there may be regions where atomic gas can cool, condense into H_2, and SF can commence (e.g. Hunt et al. 2023).

The atomic gas mass of TDGs outweighs the molecular gas mass by factors of 3–30 within the CO emitting area (see Table 1) and the stellar mass by factors of 5–15 (see table 5 in Lelli et al. 2015), so the H I centre corresponds to the centre of mass (in the case of negligible dark matter). Interestingly, PV diagrams along the CO distribution (right panels) show that there is good agreement between CO and H I line-of-sight velocities, suggesting that the two gas phases are dynamically coupled. The most likely interpretation is that molecular gas is currently forming out of atomic gas, keeping the same kinematics.

Fig. 2 compares the distribution of molecular and ionized gas, specifically the H α and H β lines that will be used to measure the SFRs. Molecular and ionized gas are roughly cospatial on kpc-scales but display different morphologies, so the spatial relation between current SF activity and molecular gas reservoir is complex. Importantly, both molecular and ionized gas are much more compact than the atomic gas and similarly displaced from the H I dynamical

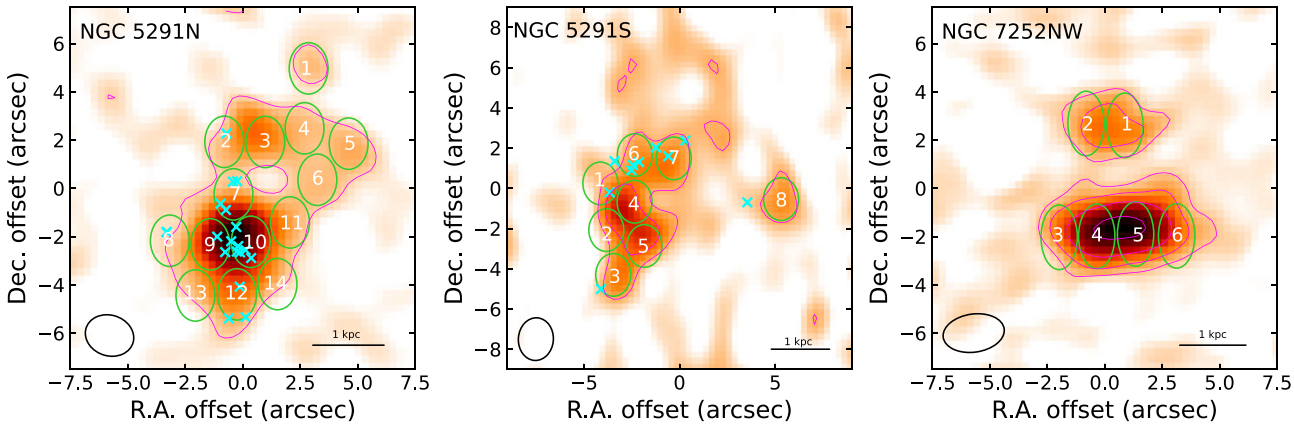

Figure 3. Integration regions for spatially resolved flux measurements in NGC 5291N (left), NGC 5291S (middle), and NGC 7252NW (right). The CO(1–0) intensity maps (red colourscale) are overlaid with the areas (green ellipses) within which integrated spectra are extracted. In NGC 5291N and NGC 5191S, the cyan crosses indicate the location of the 'secure' massive star clusters identified by Fensch et al. (2019) using *HST* images. The size of the ellipse shown in the bottom left corner is equivalent to the CO(1–0) beam. Red contours are the same as in Fig. 1.

centre. Thus, no firm statement on the large-scale dynamics of TDGs can be inferred from H α emission. The same conclusion was drawn by Lelli et al. (2015) for NGC 7252NW using H α data from GIRAFFE, which is in good agreement with the new MUSE data. On the contrary, Flores et al. (2016) inferred strong conclusions on the dynamics of the TDGs in NGC 5291 using H α data from GIRAFFE. Figs 1 and 2 show that the bright H α emission cannot be used to trace the large-scale gas kinematics of TDGs.

The H I emission appears to be the most extended and most promising tracer to probe the internal dynamics in TDGs, provided that the kinematically decoupled part can be discerned from the tidal tails and properly resolved. The H I-to-H_2 conversion and the most intense SF activity, however, do not occur exactly at the dynamical centre, possibly due to variable local conditions such as gas pressure, temperature, and volume density. A similar situation occurs in 'regular' starburst dwarfs, such as blue compact dwarfs (BCDs), which often show offsets between the peak SF activity and the dynamical centre of the galaxy (e.g. Lelli, Verheijen & Fraternali 2014b).

3.2 Emission-line measurements

We combine $\Sigma_{\rm SFR}$ traced by H α emission with $\Sigma_{\rm mol}$ traced by CO emission to investigate the spatially resolved KS relation. We define a set of independent elliptical apertures with major and minor axes matching the FWHM of the ALMA synthesized beam (see Fig. 3). We then extract integrated CO, H α, and H β spectra within each elliptical aperture from the ALMA and MUSE cubes, respectively. This is nearly equivalent to smoothing and/or re-binning the MUSE data to the lower spatial resolution of the ALMA data. The key advantage of this procedure is to ensure independent measurements of $\Sigma_{\rm SFR}$ and $\Sigma_{\rm mol}$ because the elliptical regions are equal to or larger than the angular resolution. The ellipses are chosen to cover the CO emission down to a contour with S/N = 3; for simplicity, they are oriented in the north–south direction rather than along the PA of the ALMA beam, but this choice has no appreciable effects on the final results. Using a circular aperture would also make no difference in our general results. We have 14, 8, and 6 apertures for NGC 5291N, NGC 5291S, and NGC 7252NW, respectively, for a total of 28 independent measurements.

We extract the optical and CO(1–0) spectra of each region using CASA. For each H α and H β spectra, we subtract continuum emission by calculating the mean continuum flux from two narrow spectral regions on either side of the emission profile. In all selected regions, the CO(1–0), H α, and H β lines are detected with a peak S/N ratio higher than 3.5, apart from region 8 of NGC 5291S in which H β emission is undetected. Fig. 4 shows an example of the spectra from one region in NGC 5291N.

The H α and H β lines have a nearly Gaussian shape, but the CO lines do not (see Fig. 4). Most likely, the Gaussian shape of the MUSE profiles is driven by the instrumental spectral resolution (FWHM of $\sim$80 km s^{-1} around the H α line), while the non-Gaussian shape of CO profiles is intrinsic, given the ALMA spectral resolution of $\sim$10 km s^{-1} (after Hanning smoothing). Rather than fitting a Gaussian function therefore we use direct integration to estimate the integrated flux from the emission lines of interest. The starting and ending frequency of integration were defined by visual inspection; they are typically about 100 km s^{-1} wide. In regions with low S/N, it is not trivial to identify the proper integration range. This is especially the case for the H α line because the [N II] doublet blends with the noise. In such cases, to avoid contamination from [N II] lines, we estimate the redshifted wavelength of the [N II] doublet and consider appropriate frequency ranges excluding the [N II] emission.

To extract CO spectra and measure CO fluxes, we used cubes that are *not* corrected for the ALMA primary-beam attenuation because these cubes have uniform and well-defined noise structure. In primary-beam-corrected cubes, indeed, the noise varies from pixel to pixel, so it is challenging to define the S/N ratio of the line. To recover the correct CO fluxes, instead, we use the primary-beam map and compute the average primary-beam correction within each region, then multiply the uncorrected CO flux by this value. Table 3 summarizes all our measurements.

3.3 Molecular gas masses and star formation rates

We convert the CO line flux of each region ($S_{\rm CO}\Delta v$) to a total molecular gas mass ($M_{\rm mol}$, including helium and heavier elements) assuming the Milky Way CO-to-$M_{\rm mol}$ conversion factor $\alpha_{\rm CO} = 4.3$ M$_\odot$ (K km s^{-1} pc^2)$^{-1}$ or equivalently $X_{\rm CO} = 2 \times 10^{20}$ cm^{-2} (K km s^{-1})$^{-1}$. This

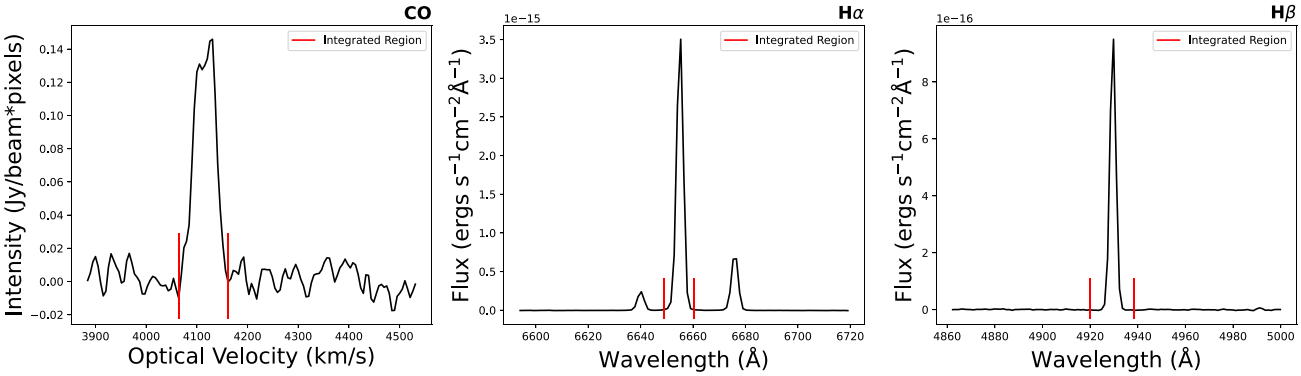

Figure 4. The CO, H α + [N II], and H β spectra of the star-forming region 9 in NGC 5291N. Red vertical lines show the range over which the spectra are integrated.

Table 3. Line fluxes, molecular masses, and SFRs within the independent regions identified in Fig. 3.

TDG	Region	$S_{CO}\,\Delta v$ (Jy km s^{-1})	M_{mol} (10^6 M$_\odot$)	$F_{H\alpha}$ (10^{-16} erg s^{-1} cm^{-2})	$F_{H\beta}$ (10^{-16} erg s^{-1} cm^{-2})	Extinction (mag)	SFR (M$_\odot$ yr^{-1})
	1	0.03	1.0	1.2	0.4	0.4	0.0006
	2	0.04	1.4	6.0	1.9	0.3	0.003
	3	0.07	2.8	4.0	1.2	0.5	0.002
	4	0.04	1.4	1.1	0.3	0.6	0.0007
	5	0.04	1.5	0.9	0.2	0.8	0.0007
	6	0.04	1.5	2.1	0.6	0.5	0.001
NGC 5291N	7	0.07	2.7	65.4	18.4	0.5	0.04
	8	0.03	1.1	15.7	4.7	0.4	0.008
	9	0.2	7.4	111.6	29.8	0.7	0.08
	10	0.2	6.5	161.2	41.1	0.8	0.1
	11	0.04	1.5	7.1	2.1	0.4	0.004
	12	0.08	3.3	66.5	17.2	0.8	0.05
	13	0.04	1.5	11.8	3.6	0.4	0.006
	14	0.03	1.3	14.1	4.2	0.4	0.007
	1	0.03	1.2	55.0	14.5	0.7	0.04
	2	0.05	1.9	21.6	6.0	0.6	0.01
	3	0.04	1.5	7.6	2.3	0.3	0.004
NGC 5291S	4	0.05	2.1	24.8	7.1	0.5	0.01
	5	0.05	2.0	4.7	1.0	1.3	0.006
	6	0.04	1.4	28.2	8.3	0.5	0.02
	7	0.04	1.6	22.7	6.5	0.5	0.01
	8	0.03	1.3	0.3	–	–	0.0001
	1	0.03	1.5	6.9	1.9	0.6	0.005
	2	0.03	1.6	1.8	0.5	0.6	0.001
NGC 7252NW	3	0.05	2.1	0.4	0.08	1.3	0.0005
	4	0.1	5.2	2.0	0.5	1.0	0.002
	5	0.1	5.3	2.0	0.4	1.3	0.003
	6	0.05	2.1	0.6	0.2	0.8	0.0006

corresponds to the following equation (Bolatto et al. 2017):

$$M_{mol} = 1.05 \times 10^4 \frac{S_{CO}\Delta v\, D_L^2}{(1+z)}, \quad (3)$$

where M_{mol} is in units of M$_\odot$, $S_{CO}\Delta v$ is in units of Jy km s^{-1}, D_L is the luminosity distance in Mpc, and z is the redshift. The choice of conversion factor in equation (3) holds for disc galaxies similar to the Milky Way. As discussed in Section 1, the same conversion factor is expected to hold in TDGs because they retain the metallicity of the parent spiral galaxies. Clearly, this is a simplifying assumption because the value of X_{CO} varies even within 'normal' disc galaxies and is known to increase with decreasing metallicity (Bolatto, Wolfire & Leroy 2013). The metallicities of our TDGs range from half solar to solar (Duc & Mirabel 1998; Lelli et al. 2015), so the variation in X_{CO} is expected to be null or small, depending on the adopted model (cf. Bolatto et al. 2013). In the worst case scenario, in some star-forming regions of our TDG sample, M_{mol} may be underestimated by a factor of ∼2–3. The molecular mass surface density (Σ_{mol}) is derived by dividing M_{mol} by the ellipse area.

The H α flux provides an instantaneous measure of the SFR as nebular emission is produced around young massive stars with masses greater than 10 M$_\odot$ and lifetimes shorter than 10–20 Myr (Kennicutt 1998a). SFR tracers probing longer time-scales have

been studied and discussed in Boquien et al. (2007, 2009, 2010). The primary contributor to systematic errors in H α-based SFRs is dust extinction, which can be accounted for by using the Balmer decrement H α/H β. We follow Bolatto et al. (2017) to estimate the nebular extinction $A_{\mathrm{H}\alpha}$:

$$A_{\mathrm{H}\alpha} = 5.86 \log \frac{F_{\mathrm{H}\alpha}}{2.86\, F_{\mathrm{H}\beta}}, \quad (4)$$

where $F_{\mathrm{H}\alpha}$ and $F_{\mathrm{H}\beta}$ are the integrated fluxes. Here, the case B recombination value of intrinsic Balmer decrement is considered to be 2.86 as suggested by Storey & Hummer (1995) for H II regions at typical electron temperatures and densities. The extinction-corrected SFR was computed as

$$\mathrm{SFR} = 7.9 \times 10^{-42}\, L_{\mathrm{H}\alpha}\, 10^{(A_{\mathrm{H}\alpha}/2.5)}, \quad (5)$$

where SFR is in units of $\mathrm{M}_\odot$ yr^{-1} and $L_{\mathrm{H}\alpha}$ is the luminosity of H α in units of erg s^{-1}. This equation assumes solar abundance and a Salpeter initial mass function (IMF) with a mass range of 0.1–100 $\mathrm{M}_\odot$ (Kennicutt 1998a). Finally, we compute Σ_{SFR} (in units of $\mathrm{M}_\odot$ yr^{-1} kpc^{-2}) dividing the SFR by the area of the region (equivalent to the beam size, see Table 2).

3.4 The Kennicutt–Schmidt relation

As a first step, we locate our three TDGs on the spatially integrated KS relation, which compares the total gas surface density (atomic plus molecular) with the SFR. We use the data from Kennicutt & Evans (2012) because they are internally self-consistent with our data: the SFRs are measured from extinction-corrected H α fluxes and the molecular gas masses assume the MW X_{CO} factor (cf. with Section 3.3). Fig. 5 shows that TDGs follow the same KS relation as 'normal' galaxies, in agreement with earlier results from Braine et al. (2001) and Boquien et al. (2011) using single-dish CO observations. Notably, if we consider only molecular gas masses, TDGs would strongly shift to the left of the relation because the total gas mass is heavily dominated by atomic gas, unlike typical spiral galaxies.

Next, we study the spatially resolved SF relation (e.g. Bolatto et al. 2017; Lin et al. 2020; Pessa et al. 2021). We compare our TDGs to 14 spiral galaxies from the ALMA-MaNGA QUEnching and STar formation (ALMaQUEST) survey (Lin et al. 2019, 2020). ALMaQUEST data represent the ideal comparison sample because (i) molecular gas masses are estimated using CO(1–0) data from ALMA as in our work, (ii) SFRs are estimated using extinction-corrected H α fluxes from IFS similar to our work, (iii) the same calibrations have been adopted (equations 3 and 5), and (iv) the angular resolution of ALMaQUEST data (∼2.5 arcsec) is similar to that of our data (∼2 arcsec) albeit the ALMaQUEST physical resolution ranges from 0.5 to 6.5 kpc depending on the galaxy distance while our physical resolution is fixed at ∼0.6 kpc. In addition, unlike other samples (Bolatto et al. 2017; Pessa et al. 2021), the ALMaQUEST data cover low gas surface densities similar to those in TDGs.

Unfortunately, we cannot study the spatially resolved SF relation considering the total gas surface densities (molecular plus atomic gas) because the angular resolution of the existing H I data of TDGs is too coarse. In fact, the entire CO emitting area is within one H I beam. The ALMaQUEST data, however, do not consider the H I surface densities as well, so our comparison in Fig. 6 is self-consistent.

Fig. 6 shows the location of TDGs on the spatially resolved SF relation from ALMaQUEST. We fit the ALMaQUEST data with a linear relation using the Markov chain Monte Carlo (MCMC) software BAYESLINEFIT (Lelli et al. 2019). The MCMC fit returns a

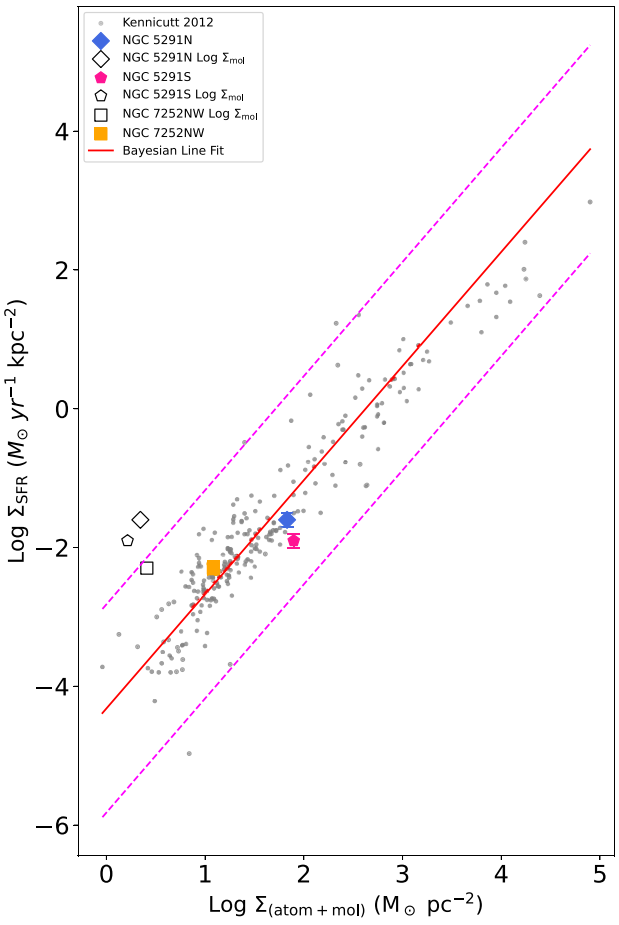

Figure 5. The location of TDGs (blue diamond, yellow square, and pink pentagon) on the spatially integrated KS relation (grey symbols, from Kennicutt & Evans 2012). The open symbols show the location of TDGs if one considers only molecular gas, neglecting atomic gas. The red line shows the best-fitting line to the data; the dashed magenta lines correspond to $\pm 3\sigma_{\mathrm{obs}}$ where σ_{obs} is the observed vertical scatter.

slope of 1.024 ± 0.008, an intercept of -2.964 ± 0.009, and a vertical observed scatter $\sigma_{\mathrm{obs}} = 0.23$ dex. The majority of TDG points (16/27) lie on the same SF relation as spiral galaxies within $\pm 3\sigma_{\mathrm{obs}}$. The correlation between Σ_{SFR} and $\Sigma_{M_{\mathrm{mol}}}$, however, is not evident when considering only TDG data. On the one hand, this occurs because most TDG points cover a small dynamic range in gas surface density (less than 1 dex) and the SF relation has substantial scatter at fixed Σ_{mol}. On the other hand, TDG data display a larger scatter from the fitted line than the ALMaQUEST data: 0.7 dex considering all TDG points and 0.4 dex considering only those within $\pm 3\sigma_{\mathrm{obs}}$. Indeed, only ∼30–35 per cent of TDG points lie within $\pm 1\sigma_{\mathrm{obs}}$ of the best-fitting relation rather than the expected 68 per cent for a Gaussian distribution.

The high scatter of TDG points may be due to small-number statistics or systematic differences between our work and the ALMaQUEST analysis. If real, instead, it could point to (i) the need of considering the total gas surface density (atomic plus molecular gas) in H I-dominated galaxies, as in the case of the spatially integrated SF relation in Fig. 5, (ii) high stochasticity in the SF history of TDGs on small spatial scales (e.g. Boquien et al. 2010), (iii) spatial variations in the X_{CO} factor due to additional effects (beyond gas metallicity) such as gas temperature, gas pressure, and UV background (e.g.

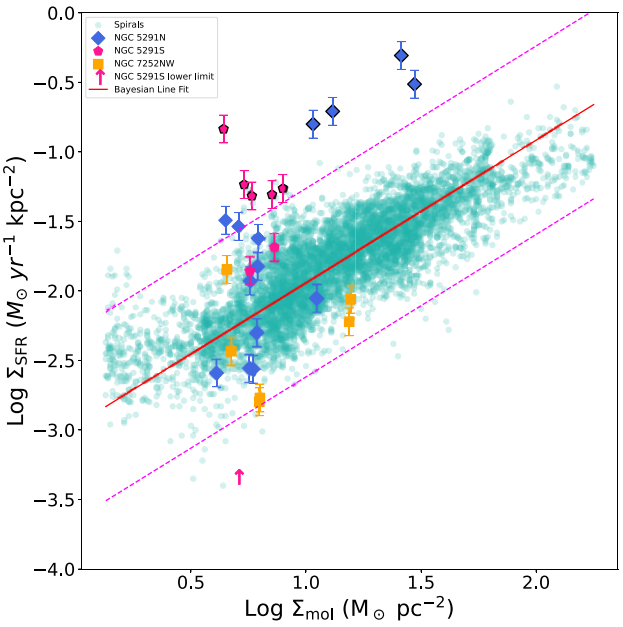

Figure 6. The location of TDGs (blue diamonds, yellow squares, and pink pentagons) on the spatially resolved KS relation from the ALMaQUEST survey (cyan circles, from Lin et al. 2019). The solid red line shows the best-fitting line to the ALMaQUEST data; the dashed magenta lines correspond to $\pm 3\sigma_{\rm obs}$ where $\sigma_{\rm obs} = 0.23$ dex is the observed vertical scatter. Symbols with a thick border correspond to regions in which young massive star clusters have been identified (see Fig. 3).

Bolatto et al. 2013), and (iv) differences in 3D volume densities due to line-of-sight integration and variable disc thickness (e.g. Bacchini et al. 2019, 2020). Given the complex evolutionary status of TDGs, which are possibly out of dynamical equilibrium (Lelli et al. 2015), it is difficult to distinguish between these possibilities.

Interestingly, a substantial fraction of TDG regions (10/28) strongly deviate from the observed SF relation and lie in the starburst zone above $+3\sigma_{\rm obs}$. These starburst regions belong to NGC 5291N and NGC 5291S. Studies with the *Hubble Space Telescope* (*HST*) show that these regions are currently forming young star clusters with masses ranging from a few 10^3 to a few 10^5 $M_\odot$ and ages from $\sim$1 to $\sim$100 Myr (Fensch et al. 2019). Thus, it is sensible that these areas have exceptionally high Star Formation Efficiencies (SFEs).

Unlike NGC 5291N and NGC 5291S, NGC 7252NW does not show starburst regions with high SFE, but most of its star-forming regions (4/6) fall below the average SF relation. Consistently, visual inspection of the available *HST* images of NGC 7252NW does not reveal any clear young star cluster. Another two TDGs with spatially resolved CO data (VCC 2062 from Lisenfeld et al. 2016 and J1023+1952 from Querejeta et al. 2021) were also found to lie systematically below the average SF relation, albeit Querejeta et al. (2021) warn that the inclusion or exclusion of diffuse CO emission (not contained in giant molecular clouds) could result into a large difference. The different behaviours shown by different TDGs may be related to the evolutionary status of the parent system and the 'age' of the specific TDG. According to numerical simulations, the gas ring around NGC 5291 was formed by a head-on galaxy collision about $\sim$360 Myr ago (Bournaud et al. 2007). On the other hand, NGC 7252 is a late-stage merger resulting from the interaction of two spiral galaxies about $\sim$700 Myr ago (Hibbard & Mihos 1995; Chien & Barnes 2010). One may speculate therefore that the TDGs around NGC 5291 are young and experiencing a period of peak SF activity due to efficient H I-to-H_2 conversion, whereas those around NGC 7252 are slightly older and more quiescent. A larger sample of TDGs around more diverse interacting systems, together with detailed numerical simulations of the system, is needed to study the relation between the interaction stage and SF activity in tidal debris.

Broadly speaking, star-forming galaxies can be classified into 'normal' and 'starbursts' using a 3σ threshold from the mean KS relation. With such a definition, starbursts represent an SF process that occurs with less than 99.7 per cent chance for a Gaussian distribution of SFEs. The star-forming regions in our TDG sample display a continuous range of SFEs, but a very large fraction of them ($\sim$ 40 per cent) proceed in starburst mode, resulting in molecular gas depletion times as short as 10–100 Myr. In the remaining $\sim$ 60 per cent of TDG regions, the SF activity proceeds in a similar way as in normal spiral galaxies, regardless of the different environmental conditions. In this sense, TDGs are 'hybrid' systems because they contain some regions behaving as normal galaxies and others as starbursts.

3.5 Time-scales and evolution of TDGs

A spatially resolved KS relation with a slope of one (as observed) implies that the molecular gas depletion time ($t_{\rm mol} = M_{\rm mol}/{\rm SFR}$) is nearly constant across spiral galaxies. Then, the intercept and observed scatter imply that $t_{\rm mol} \simeq 1 \pm 0.5$ Gyr. For our three TDGs, the molecular gas depletion times are substantially smaller: 100 Myr for NGC 5291N, 70 Myr for NGC 5291S, and 300 Myr for NGC 7252NW. The molecular gas of these TDGs therefore will soon be consumed by the SF activity unless it is replenished by efficiently converting the substantial H I reservoir into H_2 gas.

Considering the total H I mass associated with the TDG potential well (Lelli et al. 2015, their table 8), the atomic gas depletion time ($t_{\rm atom} = M_{\rm atom}/{\rm SFR}$) is about 2 Gyr for NGC 5291N, 4 Gyr for NGC 5291S, and 7 Gyr for NGC 7252NW. These values of $t_{\rm atom}$ are substantially smaller than those of low-surface-brightness (LSB) star-forming galaxies, ranging between 10 and 100 Gyr (e.g. McGaugh, Schombert & Lelli 2017), but are comparable to those of starburst dwarf galaxies (Lelli, Fraternali & Verheijen 2014a), such as BCDs. It is conceivable that both TDGs and BCDs are only able to sustain the intense SF activity for a short period of time ($\sim$0.5–1 Gyr, e.g. McQuinn et al. 2010), so the starburst will not have enough time to consume their entire H I reservoir. For example, if their SFR is going to decrease in the next 500 Myr by a factor of $\sim$10, their $t_{\rm atom}$ will increase by a similar factor, reaching the high values observed in LSB galaxies. Furthermore, there is a diffuse H I reservoir in the tidal debris around the TDGs, which might replenish their gas content.

Another interesting time-scale is the stellar mass growth time ($t_\star = M_\star/{\rm SFR}$), which we compute using the stellar masses from Lelli et al. (2015, their table 8). For NGC 7252, we find $t_\star \simeq 940$ Myr. This is larger than the dynamical time-scale of the galaxy merger ($\sim$700 Myr) inferred from numerical simulations (Chien & Barnes 2010). Assuming that the age of the TDG is equal to that of the merger, the current SFR cannot explain the present-day stellar mass: the SFR was probably higher in the past, indicating that the SF activity has been declining over time. A possible caveat is that NGC 7252NW may contain old stars from the disc of the parent galaxies, which would contribute to $M_\star$ beyond the mass formed over the past 700 Myr. In any case, the situation of NGC 5291 appears different: we find $t_\star \simeq 180$ Myr for NGC 5291N Myr and $t_\star \simeq$ 270 Myr for NGC 5291S, which are smaller than the dynamical time-scale of the galaxy collision ($\sim$360 Myr, Bournaud et al. 2007).

Thus, the current SFR can amply explain the present-day $M_\star$ of these two TDGs. These facts are in line with the speculation in Section 3.4 that the TDGs around NGC 5291 may be representative of early galaxy formation with efficient H I-to-H_2 conversion, high SFE, and short gas depletion times, while those around NGC 7252 may represent a subsequent stage with more typical SF activity. In addition, the initial conditions in the two systems may have been different: while the TDGs around NGC5291 were born out of pure gaseous condensation, those around NGC7252 may have been born in a less H I dominated environment with both gas and stars from their progenitors.

4 CONCLUSIONS

We studied the molecular and ionized gas content of three bona-fide TDGs using CO(1–0) observations from ALMA and IFS data from MUSE. For the first time, we locate TDGs on the spatially resolved KS relation. Our results can be summarized as follows:

(i) CO(1–0) and Hα emissions in TDGs are very compact and cover a much smaller area than the H I emission. Both CO and Hα lines are not suitable to study the internal kinematics of these TDGs. Most likely, molecular gas is forming out of the more extended H I disc of TDGs, having similar line-of-sight velocities.

(ii) TDGs lie on the same spatially integrated Σ_{SFR}–Σ_{gas} relation of spiral galaxies but display a substantial scatter on the spatially resolved Σ_{SFR}–Σ_{mol} relation (which neglects atomic gas due to the lack of high-resolution H I data).

(iii) The majority (60 per cent) of star-forming regions in TDGs lie on the same spatially resolved SF relation as spiral galaxies within ± 3 times the observed scatter but display a larger dispersion from the mean relation. A substantial fraction (~ 40 per cent) of star-forming regions have exceptionally high SF efficiencies, lying in the starburst regime of the KS relation. These regions belong to NGC 5291N and NGC 5291S, and are associated with the formation of massive super star clusters, which were previously identified by *HST* imaging (Fensch et al. 2019).

The growing evidence about the existence of a fundamental SF relation compels us to put the relation to test in a variety of star-forming environments. The three TDGs analysed here confirm the fundamental nature of the KS relation on subkpc scales, albeit regions with exceptionally high SF efficiencies do exist. Future studies may investigate the spatially resolved KS relation in other bona-fide TDGs, probing even more diverse star-forming environments, such as younger and/or older tidal debris.

DATA AVAILIABILITY

The raw data used in this work are available in the ALMA and ESO archives. Reduced data are available on request.

ACKNOWLEDGEMENTS

We are grateful to the anonymous referee for the useful comments that helped to improve the paper. We thank Rob Kennicutt and Lin Li-Hwai Lin for providing the KS relation data in tabular form. NK and FL thank the School of Physics and Astronomy of Cardiff University, where this work started as part of a Master thesis project. NK acknowledges support from the Programa de doctorado en Astrofísica y Astroinformática of Universidad de Antofagasta. MB acknowledges support from FONDECYT regular grant 1211000 and by the ANID BASAL project FB210003. UL acknowledges support by the research projects AYA2017-84897-P and PID2020-114414GB-I00 from the Spanish Ministerio de Economía y Competitividad, from the European Regional Development Funds (FEDER) and the Junta de Andalucía (Spain) grant FQM108. This paper makes use of the following ALMA data: ADS/JAO.ALMA#2015.1.00645.S. ALMA is a partnership of ESO (representing its member states), NSF (USA), and NINS (Japan), together with NRC (Canada), MOST and ASIAA (Taiwan), and KASI (Republic of Korea), in cooperation with the Republic of Chile. The Joint ALMA Observatory is operated by ESO, AUI/NRAO, and NAOJ. Based on observations collected at the European Organisation for Astronomical Research in the Southern Hemisphere under ESO MUSE program 60.A-9320(A) and 097.B-0152(A). Based on public data released from the MUSE WFM-AO commissioning observations at the VLT under Programme IDs 60.A-9100 runs G & H.

REFERENCES

Bacchini C., Fraternali F., Iorio G., Pezzulli G., 2019, A&A, 622, A64
Bacchini C., Fraternali F., Pezzulli G., Marasco A., 2020, A&A, 644, A125
Barnes J. E., Hernquist L. E., 1991, ApJ, 370, L65
Barnes J. E., Hernquist L., 1992, Nature, 360, 715
Bigiel F., Leroy A., Walter F., Brinks E., De Blok W., Madore B., Thornley M. D., 2008, AJ, 136, 2846
Bigiel F., Leroy A., Walter F., Blitz L., Brinks E., de Blok W. J. G., Madore B., 2010, AJ, 140, 1194
Bolatto A. D., Wolfire M., Leroy A. K., 2013, ARA&A, 51, 207
Bolatto A. D. et al., 2017, ApJ, 846, 159
Boquien M., Duc P. A., Braine J., Brinks E., Lisenfeld U., Charmandaris V., 2007, A&A, 467, 93
Boquien M. et al., 2009, AJ, 137, 4561
Boquien M., Duc P. A., Galliano F., Braine J., Lisenfeld U., Charmandaris V., Appleton P. N., 2010, AJ, 140, 2124
Boquien M., Lisenfeld U., Duc P. A., Braine J., Bournaud F., Brinks E., Charmandaris V., 2011, A&A, 533, A19
Borne K. D., Richstone D. O., 1991, ApJ, 369, 111
Bournaud F., Duc P. A., Amram P., Combes F., Gach J. L., 2004, A&A, 425, 813
Bournaud F. et al., 2007, Science, 316, 1166
Braine J., Duc P.-A., Lisenfeld U., Charmandaris V., Vallejo O., Leon S., Brinks E., 2001, A&A, 378, 51
Chien L.-H., Barnes J. E., 2010, MNRAS, 407, 43
Duc P.-A., Mirabel I., 1998, A&A, 333, 813
Duc P.-A., Bournaud F., Boquien M., 2006, in Elmegreen B. G., Palous J., eds, Proc. IAU Symp 237, riggered Star Formation in a Turbulent ISM. Cambridge Univ. Press, Cambridge, p. 323
Ellison S. L., Mendel J. T., Patton D. R., Scudder J. M., 2013, MNRAS, 435, 3627
Ellison S. L., Thorp M. D., Pan H.-A., Lin L., Scudder J. M., Bluck A. F. L., Sánchez S. F., Sargent M., 2020, MNRAS, 492, 6027
Elmegreen B., Kaufman M., Thomasson M., 1993, ApJ, 412, 90
Fensch J., Duc P. A., Weilbacher P. M., Boquien M., Zackrisson E., 2016, A&A, 585, A79
Fensch J. et al., 2019, A&A, 628, A60
Flores H., Hammer F., Fouquet S., Puech M., Kroupa P., Yang Y., Pawlowski M., 2016, MNRAS, 457, L14
Hibbard J. E., Mihos J. C., 1995, AJ, 110, 140
Hibbard J., Guhathakurta P., Van Gorkom J., Schweizer F., 1994, AJ, 107, 67
Hunt L. K. et al., 2023, A&A, 675, A64
Kennicutt R. C., Jr, 1998a, ARA&A, 36, 189
Kennicutt R. C., Jr, 1998b, ApJ, 498, 541
Kennicutt R. C. J., Evans N. J., 2012, ARA&A, 50, 531
Lelli F., Fraternali F., Verheijen M., 2014a, A&A, 563, A27
Lelli F., Verheijen M., Fraternali F., 2014b, A&A, 566, A71
Lelli F. et al., 2015, A&A, 584, A113

Lelli F., McGaugh S. S., Schombert J. M., Desmond H., Katz H., 2019, MNRAS, 484, 3267
Leroy A. K., Walter F., Brinks E., Bigiel F., De Blok W., Madore B., Thornley M., 2008, AJ, 136, 2782
Lin L. et al., 2019, ApJ, 884, L33
Lin L. et al., 2020, ApJ, 903, 145
Lisenfeld U., Braine J., Duc P., Boquien M., Brinks E., Bournaud F., Lelli F., Charmandaris V., 2016, A&A, 590, A92
Longmore A., Hawarden T., Cannon R., Allen D., Mebold U., Goss W., Reif K., 1979, MNRAS, 188, 285
McGaugh S. S., Schombert J. M., Lelli F., 2017, ApJ, 851, 22
McMullin J. P., Waters B., Schiebel D., Young W., Golap K., 2007, in Shaw R. A., Hill F., Bell D. J., eds, ASP Conf. Ser. Vol. 376, Astronomical Data Analysis Software and Systems XVI. Astron. Soc. Pac., San Francisco, p. 127
McQuinn K. B. W. et al., 2010, ApJ, 724, 49
Malphrus B. K., Simpson C. E., Gottesman S., Hawarden T. G., 1997, AJ, 114, 1427
Mirabel I. F., Dottori H. A., Lutz D., 1992, A&A, 256, L19
Pessa I. et al., 2021, A&A, 650, A134
Querejeta M. et al., 2021, A&A, 645, A97
Renaud F., Bournaud F., Kraljic K., Duc P. A., 2014, MNRAS, 442, L33
Roychowdhury S., Chengalur J. N., Kaisin S. S., Karachentsev I. D., 2014, MNRAS, 445, 1392
Roychowdhury S., Huang M.-L., Kauffmann G., Wang J., Chengalur J. N., 2015, MNRAS, 449, 3700
Schmidt M., 1959, ApJ, 129, 243
Storey P., Hummer D., 1995, MNRAS, 272, 41
Weilbacher P. M. et al., 2020, A&A, 641, A28
Zwicky F., 1956, Ergebnisse der exakten Naturwissenschaften, 29, 344

This paper has been typeset from a TEX/LATEX file prepared by the author.